Magnetic properties, critical behavior and magnetocaloric effect in the nanocrystalline Pr_2Fe_1_6Al

Hamdi Jaballah, Rim Guetari, N. Mliki, Lotfi Bessais

Magnetic properties, critical behavior and magnetocaloric effect in the nanocrystalline $Pr_2Fe_{16}Al$.

H. Jaballah,[1,2,*] R. Guetari,[1,†] N. Mliki,[2,‡] and L. Bessais[1,§]

[1] *Univ Paris Est Creteil, CNRS, ICMPE, UMR 7182, 2 rue Henri Dunant, F-94320 Thiais, France*
[2] *Université de Tunis El Manar, Faculté des Sciences de Tunis, Lab Mat Org & Propriétés LR99ES17, Tunis 2092, Tunisia.*

(Dated: May 1, 2024)

We report the correlation between critical behavior and magnetocaloric effect around magnetic phase transition temperature, using magnetization isotherms of $Pr_2Fe_{16}Al$. We used four techniques to determine the critical exponents: the Modified Arrott plot, Kouvel-Fisher plot, critical isotherm technique, and magnetocaloric effect method. The critical exponents values for $Pr_2Fe_{16}Al$ are similar to that found by the 3D-Heisenberg model. The validity and the reliability of our critical exponents were confirmed. The isotherm $M(H)$ curves below and above the critical temperatures collapse into two independent universal branches with the found critical exponents. The exponents determined in this study are close to those calculated from the results of the renormalization group approach for a heuristic model of three-dimensional Heisenberg ($d = 3, n = 3$). A correlation between critical behavior and magnetocaloric effect is demonstrated.

PACS numbers: 75.50.Bb, 75.50.Tt, 76.80.+y
Keywords: Intermetallic, magnetocaloric compounds; ferro-paramagnetic transition; Critical behavior.

I. INTRODUCTION

Intermetallic (R-M) compounds combine the large magnetocrystalline anisotropy of rare-earth (R) atoms, the high magnetization transition and high Curie temperature of metal (M) atoms have attracted great interest due to their wide applications. R-M compounds have been investigated in various works on their thermodynamic properties [1], thermal hysteresis [2], hydrogen absorption [3, 4], thermal expansion properties and magnetocaloric effect (MCE) [5–7]. Recently, many R-M-based intermetallics and oxide compounds have been reported to exhibit promising magnetocaloric performance at low temperatures [8–15]. Moreover, a great interest has been given to the study of critical behavior in intermetallic compounds in the vicinity of Curie temperature [16–21]

Among the intermetallics containing rare earth and a transition metal, we are interested in R_2M_{17}. According to structural investigations, there are two possible structure for R_2M_{17} series, the hexagonal Th_2Ni_{17} ($P6_3mmc$-space group) and the rhombohedral Th_2Zn_{17} ($R\bar{3}m$-space group) depending to the rare earth or metal transition [22]. Among them, we are interested in Pr_2Fe_{17} based materials. Pr_2Fe_{17} crystallizes in $R\bar{3}m$-space group. The rare-earth atom possesses one crystallographic site in this structure, but the iron atom possesses four sites: $6c, 18f, 18h$, and $9d$. The principal parameters that can influence the exchange interaction are The magnetic moment of the transition metal atom, the de Gennes factor, and inter-atomic distances. Investigation of thermomagnetic properties shows that the Curie temperatures of Pr_2Fe_{17} are shallow compared to other R-T compounds. Exchange interactions cause the ferromagnetic state in R-M compounds; the Curie temperature increases when the exchange interactions increase. Morrish *et al.* were calculated the exchange integrals of each iron site. Indeed, they found that exchange integrals between two iron atoms are negative for an inter-atomic distance less than 2.45 Å. This result is the origin of the relatively low value of Curie temperature in Pr_2Fe_{17} [23]. $Pr_2Fe_{16}Al$ compound exhibits a second-order magnetic phase transition and crystallizes in the same space group with Pr_2Fe_{17} [24]. In the case of second-order magnetic phase transition, the macroscopic thermodynamic quantities follow a power law in the vicinity of Curie temperature, a set of critical exponents characterizes these laws; they are still valid even over the area of critical fluctuations. We interest in this study in $Pr_2Fe_{16}Al$ compound. These systems have interesting magnetic properties; their Curie temperature and magnetization amplitude are easily controlled with the substitution in the rare-earth site and a transition metal. Therefore, they can be interesting for applications like magnetic refrigeration, magnetic recording, and hydrogen storage. Moreover, it is always essential to study them not only because of their potential applications but also for understanding the fundamental properties of these materials. In this research, we studied the correlation between critical behavior and magnetocaloric effect near the Curie temperature, the nature as well as the range of interaction in $Pr_2Fe_{16}Al$ samples.

* Corresponding author. H. Jaballah, Univ Paris Est Creteil, CNRS, ICMPE, UMR 7182, 2 rue Henri Dunant, F-94320 Thiais, France. E-mail address: hamdi.jaballah@u-pec.fr
† rim.guetari@glvt-cnrs.fr
‡ najeh.mliki@fst.utm.tn
§ bessais@cnrs.fr

II. EXPERIMENTS

$Pr_2Fe_{16}Al$ was prepared from high purity elements praseodymium (Pr) 99.98%, aluminium (Al) 99.9%, and iron(Fe) 99.9% by arc-melting technique under a purified argon atmosphere. The elements are placed in a copper crucible cooled by cold water. The ingot was then subsequently processed into nanopowders by undergoing high energy ball milling for 5 hours in Ar atmosphere, using a Fritsch P7 planetary mill. the powder is wrapped into tantalum foil and introduced into a silica tube sealed under secondary vacuum 2×10^{-6} bar [25, 26]. The ingot is heat-treated for 30 min at 1073 K and finally, water quenched [27, 28]. Phase analysis has been performed by X-ray powder diffraction (XRD), using D8 Brucker diffractometer with Cu Kα radiation $\lambda = 1.54178$ Å. XRD data of the samples have been collected between 20° and 80° at room temperature with 0.015 step width. XRD diagrams are analyzed with the Rietveld method [29, 30] using the Fullprof program [31, 32].A Physical Properties Measurement System (PPMS) magnetometer is used for measurements at low temperatures. Isotherms are collected at an interval of 1 K around T_C with an applied magnetic field up to 5 T. To get the internal field H_{int} H_{int}=H_{ext}-N_{Demag}M(T, H_{ext}), where M is the measured magnetization, the external applied magnetic field H_{ext} has been corrected for the demagnetization effect. Demagnetization constant N_{Demag} has been determined from M vs H_{ext} curve in low field region following the method given in Ref [33].

III. RESULTS AND DISCUSSIONS

A. Structure and Magnetic properties

Fig. 1 shows the Rietveld refinement of the XRD data of the sample $Pr_2Fe_{16}Al$ milled and annealed at 1273 K. XRD patterns of $Pr_2Fe_{16}Al$ and the compound is presented with Rietveld refinement in Fig. 1. The pure Pr_2Fe_{17} compound crystallizes in a rhombohedral structure of the Th_2Zn_{17} type in the space group $R\bar{3}m$. In this structure, Pr atoms occupy 6c sites, while (Fe,Al) atoms occupy four different crystallographic sites which are: $18f, 18h, 6c$ and $9d$ (in Wyckoff notation).

The refinement revealed that the Th_2Zn_{17} type phase of space group $R\bar{3}m$ is more than 98 % majority.

Tab. I shows unit cell parameters values, atomic positions of all Wyckoff sites R_B and χ^2 factor. Similar lattice parameter values and atom positions were found in the previous work [34, 35].

Fig. 2 shows The magnetization variation with temperature for $Pr_2Fe_{16}Al$ compound measured under an external applied field of 0.1 T. Curie temperature is identified as the temperature that corresponds to the minimum of dM/dT curve. For Pr_2Fe_{17}, Curie temperature is equal to 285 K [36]. After substitution of iron by an Aluminium atom, the value of Curie temperature increased significantly from 285 K to 356 K, the same behavior was observed by Guetari *et al.* [24].

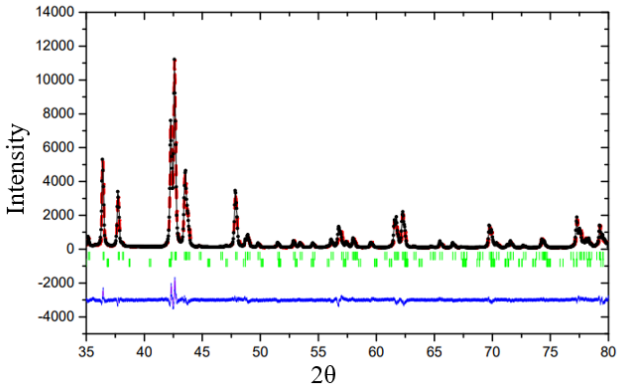

Figure 1. XRD of the compound $Pr_2Fe_{16}Al$ milled and annealed at 1273 K for 30 min. The black and red line presents respectively the calculated intensities and the experimental intensities. The green vertical bars correspond to (hkl) line positions (Positions of Bragg peaks). The blue line shows the difference between the calculated and experimental intensities.

Table I. a and c unit cell parameters, R_B, χ^2 factors, and atomic positions from Rietveld refinement of $Pr_2Fe_{16}Al_1$.

a (Å)	8.6193 (2)
c (Å)	12.5165 (4)
c/a	1.452
V (Å^3)	795
χ^2	2.08
R_B	4.103
$x\{18f\}$(Fe)	0.284(2)
$x\{18h\}$(Fe)	0.504(3)
$z\{6c\}$(Pr)	0.347(4)
$x\{6c\}$(Fe)	0.096(2)
$z\{18h\}$(Fe)	0.158(2)

In R-M compounds, the Curie temperature corresponds to a direct measure of the exchange interaction. This interaction depends strongly on the magnetic moment of the transition metal atom and the distance between near-neighbors. Because of the magnetic dilution for $Pr_2Fe_{17-x}Al_x$, the significant increase of T_C value can not be explained only by the magnetic moment of transition metal. However, it has been demonstrated that unit cell parameters of Pr_2Fe_{17} increase with Al content, due to the fact that r_{Al} (1.43 Å) > r_{Fe} (1.27 Å) and consequently Fe-Fe atomic distances increase [24]. Morrish *et al.* have demonstrated by fitting the hyperfine field of all iron sites ($6c, 9d, 18h$ and $18f$) at different temperatures in Sm_2Fe_{17} the dependence of exchange integrals value on the interatomic Fe-Fe distances. They found that there is a coexistence of negative and positive interactions in

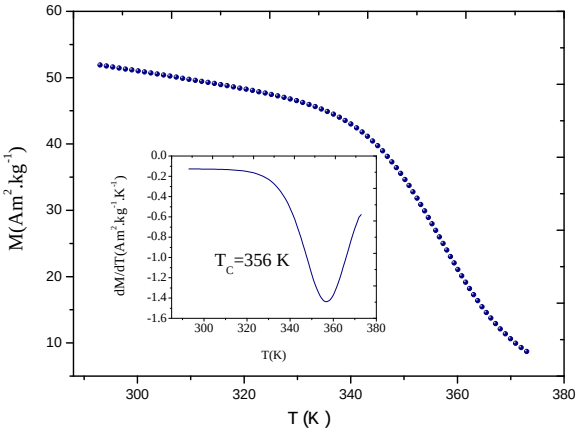

Figure 2. Magnetization plotted against temperature at $\mu_0 H$ =0.1 T with dM/dT for $Pr_2Fe_{16}Al$.

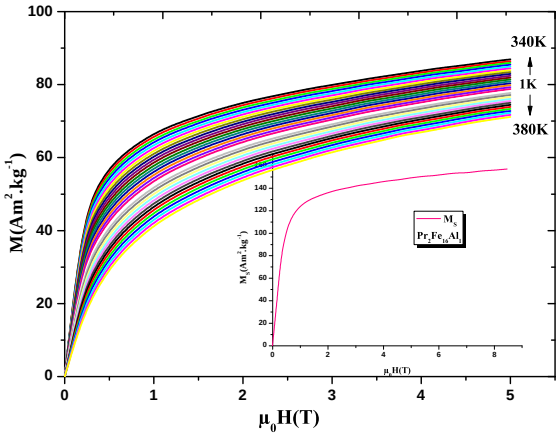

Figure 3. Isotherms $M(H)$ measured between 340 and 380 K under an applied magnetic field 0 - 5 T for $Pr_2Fe_{16}Al$.

Sm_2Fe_{17} [23]. A slight increase of distance between pairs of iron leads to a large increase in the amplitude of exchange integrals, consequently a significant increase of Curie temperature value. Combining the result found by Morrish *et al.* and the increase of Fe-Fe distance, we can explain the significant increase of Curie temperature by the magnetovolume effect. Another important factor responsible for the increase of T_C is the electronic effect. It has been demonstrated that the increase of Co content in $Sm_2Fe_{17-x}Co_x$ leads to an increase of the hyperfine field, which is explained by the increase of core electron polarization due to the asymmetric filling of 3d band by the additional electron of Co atom [37]. Based on this argument, the additional electron of the Al atom can be responsible for the evolution of T_C. Finally, the coexistence of the two important competitive factors, magnetovolume effect, and electronic effect, can be responsible for the increase of T_C.

Isothermal magnetization $M(\mu_0 H, T)$ curves measured at different magnetic fields between 0 and 5 T and temperatures from 340 to 380 K with ΔT=1 K is shown in Fig. 3. It shows that, for temperatures lower than T_C, which corresponds to a ferromagnetic state, the magnetization increases notably with the magnetic field. However, the material is paramagnetic for temperatures higher than T_C, and the magnetization increases slowly with the applied magnetic field. We also note that the magnetization decreases when the temperature increases for a given magnetic field.

B. Critical study

1. *Modified Arrott plot method*

We plotted the Arrott plots $M^2 = f(H/M)$ deduced from isotherm magnetization $M(H)$ curves (Fig. 3). From the shape and the slope of the curves, we can determine the type of the phase transition [38]: If the slope is negative and the Arrott plots close to the Curie temperature have the S shape, the transition from the ferromagnetic state to the paramagnetic state is, therefore, a first-order transition. If the curves have a single inflection point and a positive slope, the transition from the ferromagnetic state to the paramagnetic one is a second-order transition. Fig. 3 shows a positive slope which indicates that $Pr_2Fe_{17}Al$ exhibits a second-order one. To determine the critical exponents and the Curie temperature, an Arrott plot method is used [39]. Arrott plot supposes that $\beta = 0.5$ and $\gamma = 1.0$, which correspond to the critical exponents of mean-field model [39]. Based on this method, isotherms plotted in the form of M^2 vs H/M show in the high field region linear behavior with the same slope, and the isotherm at the critical temperature T_C should pass through the origin. Fig. 4 shows downward curvature also in the high region field; this means that the mean-field model is not the suitable model for our compound.

The modified Arrott plot of $M^{1/\beta}$ vs $(H/M)^{1/\gamma}$ is used in order to determine the most appropriate model for $Pr_2Fe_{16}Al$ sample [40]. The Arrott-Noakes equation of state gives it:

$$(H/M)^{1/\gamma} = p\epsilon + qM^{1/\beta} \quad (1)$$

Where p and q are constants, and $\epsilon = (T - T_C)/T_C$ is the reduced temperature. Three kinds of possible exponents belonging to 3D Heisenberg model ($\beta = 0.365, \gamma = 1.386$), 3D Ising model ($\beta = 0.325, \gamma = 1.241$) and tricritical mean-field model ($\beta = 0.25, \gamma = 1.0$) are used to construct the modified Arrott plot [41], Fig. 7 shows that all curves exhibit a linear behavior, but, it is easy to see that isotherms curve are not parallel to each other, as a result, the tricritical mean field is not the suitable model

for our compound. All curves in Fig. 5 and Fig. 6 show a linear behavior with a quasi-parallel isotherms curve; this indicates that the 3D-Ising or 3D-Heisenberg model can be the suitable model for our compound. We used the normalized slope (NS) in order to determine the most appropriate model for our compound, it is defined as $N_S = S(T)/S(T_c)$ where $S(T) = dM^{1/\beta}/d(H/M)^{1/\gamma}$, For the most adequate model, the modified Arrott plot should be a series of parallel lines in the high-field region with the same slope, consequently $N_S = S(T)/S(T_c) \sim 1$. Fig. 8 shows that the deviation from $N_S = S(T)/S(T_c) = 1$ is more notable for 3D-Ising model than 3D-Heisenberg one.

To determine with more precision the critical exponents β, γ, an iterative method has been used[42]. $M_s(T)$ and $\chi_0^{-1}(T)$ are determined by a linear extrapolation of the high field region, in fact, $M_s(T)$ and $\chi_0^{-1}(T)$ correspond to the intercept of extrapolated straight lines with $M^{1/\beta}$ and $(H/M)^{1/\gamma}$ axis, respectively.

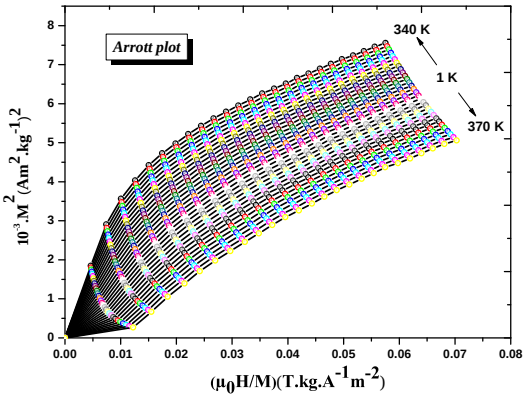

Figure 4. Arrott plot for $Pr_2Fe_{16}Al$.

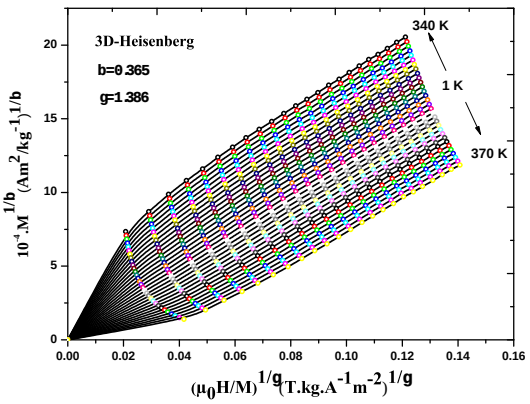

Figure 5. Modified Arrott plot using 3D-Heisenberg model exponents $Pr_2Fe_{16}Al$

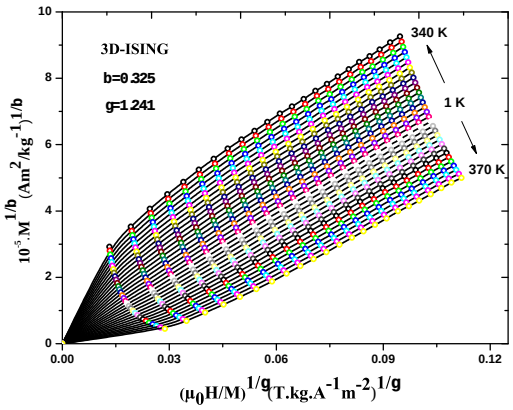

Figure 6. Modified Arrott plot using 3D-Ising model exponents $Pr_2Fe_{16}Al$

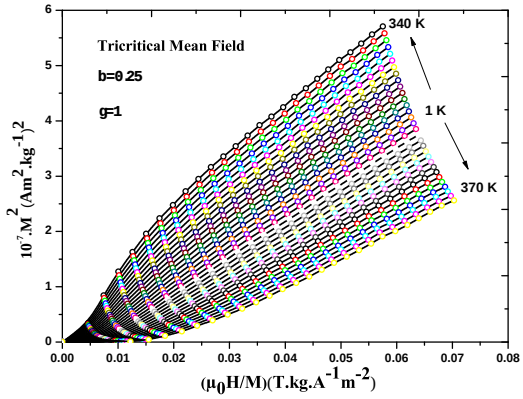

Figure 7. Modified Arrott plot using tricritical mean field model exponents $Pr_2Fe_{16}Al$.

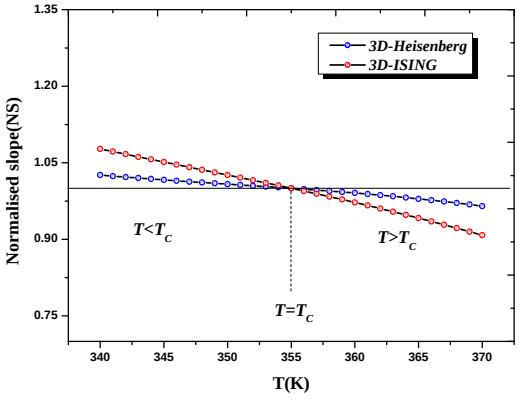

Figure 8. The normalized slopes plotted against temperature around T_C for $Pr_2Fe_{16}Al$.

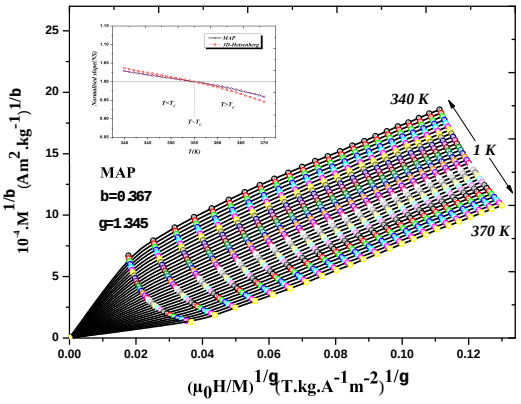

Figure 9. Modified Arrott plot of $Pr_2Fe_{16}Al$.

A set of β and γ can be obtained by fitting the data following the Eq. (2) and Eq. (3), which are given by the following relation:

$$M_s(T) = M_s(0)(-\epsilon)^{\beta}, \epsilon < 0, T < T_C \quad (2)$$

$$\chi_0^{-1}(T) = \chi_0^{-1}(0)(\epsilon)^{\gamma}, \epsilon > 0, T > T_C \quad (3)$$

where $M_s(0)$ and $\chi_0^{-1}(0)$ are the critical amplitudes and $\epsilon = (T - T_C)/T_C$ is the reduced temperature [43].

Then a new modified Arrott plot is constructed using the new values of β and γ. As a result, new $M_s(T)$ and $\chi_0^{-1}(T)$ are generated from the linear extrapolation from the high-field region. Consequently, new β and γ can be obtained. This procedure was repeated until the values of β, and γ became unchanged. Fig. 10 present

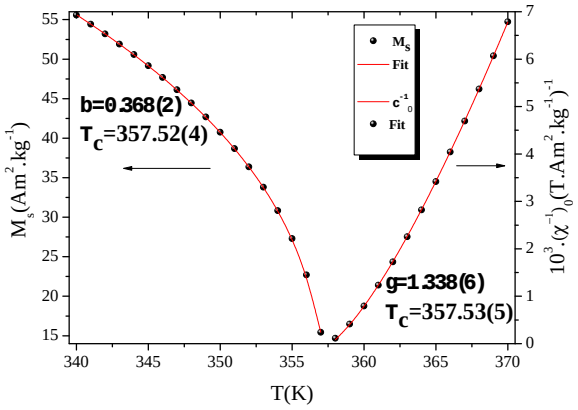

Figure 10. The spontaneous magnetization $M_s(T)$(left) and the inverse of initial susceptibility $\chi_0^{-1}(T)$ (right) plotted against temperature for $Pr_2Fe_{16}Al$. The solid lines represent the fit.

the final $M_s(T)$ and $\chi_0^{-1}(T)$ with solid fitting curves. The values of critical exponents β and γ and value of T_C are obtained.

2. *Kouvel Fisher method*

Kouvel-Fisher method is used in order to determine with more precision the values of β and γ [44]:

$$M_s(T)/(dM_s(T)/dT) = (T - T_C)/\beta$$

$$\chi_0^{-1}(T)/(d\chi_0^{-1}(T)/dT) = (T - T_C)/\gamma$$

Based on this method, $\chi_0^{-1}(T)/(d\chi_0^{-1}(T)/dT)$ and $M_s(T)/(dM_s(T)/dT)$ are a linear functions of temperature with slopes of $1/\gamma$ and $1/\beta$, respectively. They intercept temperature axis for T=T_C. As shown in Fig. 11, the linear fits give β with T_C and γ with T_C Tab. II.

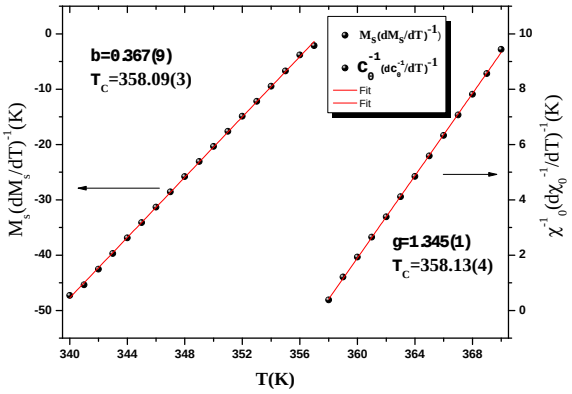

Figure 11. (b) Kouvel-Fisher plots of $M_s(T)/(dM_s(T)/dT)$ (left) and $\chi_0^{-1}(T)/(d\chi_0^{-1}(T)/dT)$ (right) for $Pr_2Fe_{16}Al$. The red solid lines represents the fit

The third exponent δ has been calculated using Widom scaling law as follow:

$$\delta = 1 + \gamma/\beta$$

. β and γ values determined from the modified Arrott plot and Kouvel-Fisher plot were used to deduce δ values (Tab II).

3. *Isotherm method*

Fig. 12 shows the isotherm magnetization M(H) at T_C, with the inset plotted on a log-log scale. δ value is deduced from the fitting of the critical isotherm using the following equation:

$$M = DH^{1/\delta}, \epsilon = 0, T = T_C \quad (4)$$

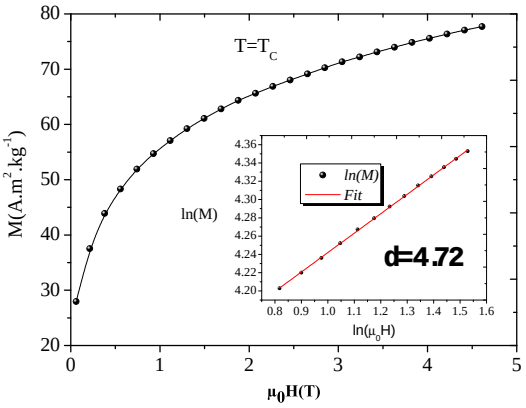

Figure 12. The isothermal magnetization curve againt applied magnetic field at T_C for $Pr_2Fe_{16}Al$ sample. The inset shows the same plot in logarithmic scale.

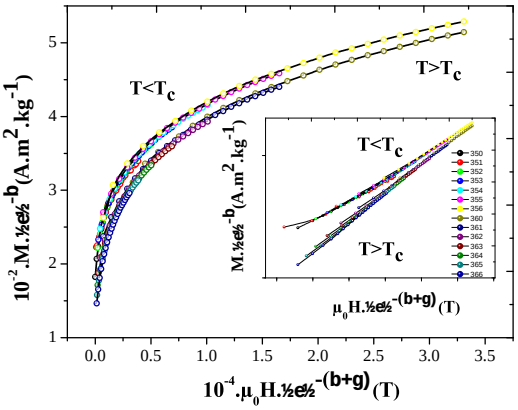

Figure 13. Scaling plots below and above T_C for $Pr_2Fe_{16}Al$ sample. The inset shows the same plot in logarithmic scale.

Where D is the critical amplitude [43]. δ=4.72 was determined based on the fit of the critical isotherm, it is close to the values deduced from the modified Arrott plot and Kouvel-Fisher plot. The critical exponents $Pr_2Fe_16Al_1$ samples are close to critical exponents of 3D-Heisenberg with a slight deviation.

4. *Validity of critical exponents*

We verify the validity and the reliability of the founded critical exponents based on the scaling hypothesis:

$$M(H,\epsilon) = \epsilon^{\beta} f_{\pm}(H/\epsilon^{\beta+\gamma}) \tag{5}$$

where f_- for $T < T_C$ and f_+ for $T > T_C$ are the regular functions. By writing magnetization and magnetic field in these renormalized forms, renormalized magnetization $m \equiv \epsilon^{-\beta} M(H,T)$ and renormalized field $h \equiv \epsilon^{-\beta+\gamma} H$, Eq. (5) can be written as:

$$m = f_{\pm}(h) \tag{6}$$

m and h is an important criterion to check the validity of the found critical exponents. Eq. (5) implies that for an appropriate values of β, γ, and δ, we obtain tow universal branches one below Curie temperature and the second above Curie temperature.

Fig. 13 and Fig. 14 show that the renormalised isotherms collapse into independent universal branches, which means that the selected critical exponents β, γ, and δ are valid.

The obtained critical exponents of $Pr_2Fe_{16}Al$ exhibit a slight deviation from 3D-Heisenberg model, they are listed in Tab II for comparison.

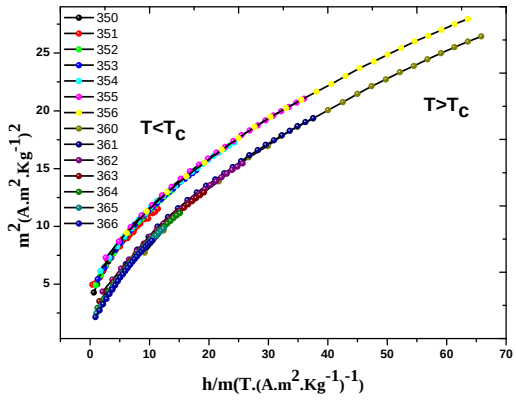

Figure 14. The renormalized magnetization (m^2) plotted against renormalized field (h/m) for $Pr_2Fe_{16}Al$ sample.

Table II. Values of critical exponents determined from the modified Arrott plot, Kouvel-Fisher plot, the critical isotherm and MCE method are given for $Pr_2Fe_{16}Al$. The theoretically predicted values of critical for comparison.

	Ref.	Technique	β	γ	δ
b	This Work	MAP	0.368(2)	1.338(6)	4.619(3)
	-	KF	0.367(9)	1.345(1)	4.665 (6)
	-	CI	-	-	4.72 (2)
	-	MCE	0.350(2)	1.316(6)	4.76 (2)
M-F	[41]	Theory	0.5	1	3
3D-H	[41]	Theory	0.365	1.386	4.79
3D-I	[41]	Theory	0.325	1.241	4.82

5. Effective critical exponents

In view of the deviation of the deduced exponents in present study from the conventional theoretical values, it is important to clarify whether $Pr_2Fe_{16}Al$ compound belongs to any universality class as they approach the asymptotic limit. For this purpose, we introduce effective critical exponents β_{eff} and γ_{eff}, they are calculated using Eq. (7) and Eq. (8) [44].

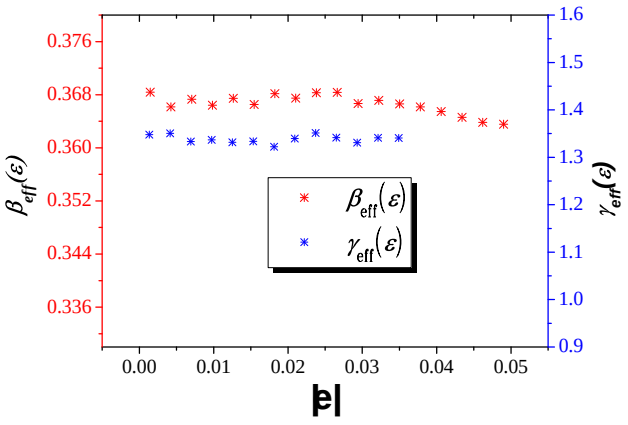

Figure 15. The effective exponents plotted against the reduced temperature ϵ for $Pr_2Fe_{16}Al$ sample.

$$\beta_{eff}(\epsilon) = \frac{dln(M_s(\epsilon))}{dln(\epsilon)} \tag{7}$$

$$\gamma_{eff}(\epsilon) = \frac{dln(\chi_0^{-1}(\epsilon))}{dln(\epsilon)} \tag{8}$$

β_{eff} and γ_{eff} vs ϵ curve show a monotonic change even in the asymptotic critical region. A nonmonotonic change of effective exponents with ϵ can be explained by: (I) System goes through crossover regime to another universality class in asymptotic regime [45], (II) ϵ_{min} is not falling in the asymptotic regime and T_C must be approached more nearly to have asymptotic exponents and (III) ϵ_{min} is in the asymptotic region, it was observed in disordered materials in asymptotic regime that effective exponents does not match with the universality classes [46]. For $Pr_2Fe_{16}Al$ the monotonic changes of β_{eff} and γ_{eff} with reduced temperature is attributed to magnetic orders. In the critical region when $T \sim T_C$ ($\epsilon \longrightarrow 0$), effective exponents $\beta_{eff}(\epsilon)$ and $\gamma_{eff}(\epsilon)$ should $\sim$ to real exponents value β and γ. Around Curie temperature ($\epsilon \longrightarrow 0$), we found ($\beta_{eff}$=0.368, γ_{eff}=1.347) for $Pr_2Fe_{16}Al$, which approach to critical exponents observed experimentally (see Tab II).

6. Magnetocaloric effect method

To determine the MCE in the magnetic material $Pr_2Fe_{16}Al$, we calculate the variation of the magnetic entropy change produced after the application of a magnetic field with the following Maxwell relation:

$$\Delta S_{\mathrm{M}} = \mu_0 \int_0^H \left(\frac{\partial M}{\partial T}\right)_H dH$$

Where M is the magnetization, T is the temperature and H is the applied magnetic field. However, if the isothermal $M(H)$ curves are measured by discrete field changes the following expression might be used [47]:

$$|\Delta S_{\mathrm{M}}| = \mu_0 \sum_i \frac{M_i - M_{i+1}}{T_{i+1} - T_i} \Delta H_i$$

Magnetic cooling efficiency is estimated by considering the magnitude of magnetic entropy change (ΔS_M^{max}), and its full-width at half-maximum (δT^{FWHM}) [48]. A product of ΔS_M^{max} and δT^{FWHM} is called relative cooling power (RCP) based on magnetic entropy change and can be calculated by:

$$RCP = \Delta S_M^{max}.\delta T^{FWHM} \tag{9}$$

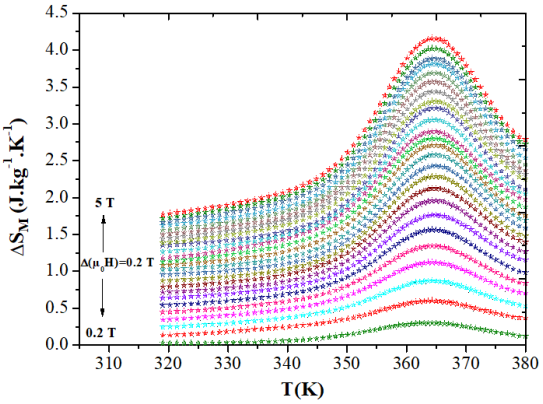

Figure 16. The magnetic entropy change plotted against temperature for $Pr_2Fe_{16}Al$ compound at several applied magnetic field.

Universal phenomenological curve using normalized entropy change $-\Delta S/-\Delta S_{\mathrm{max}}$ as a function of rescaled temperature can be obtained for materials that exhibit a second-order magnetic phase transition from the ferromagnetic to the paramagnetic state. [49].

$$\Theta = -(T - T_{\mathrm{C}})/(T_{\mathrm{r1}} - T_{\mathrm{C}}), T \leq T_{\mathrm{C}}$$

$$\Theta = (T - T_{\mathrm{C}})/(T_{\mathrm{r2}} - T_{\mathrm{C}}), T \geq T_{\mathrm{C}}$$

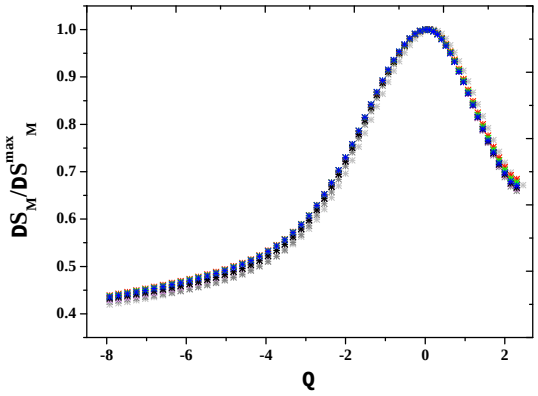

Figure 17. Normalized magnetic entropy change plotted against reduced temperature for $Pr_2Fe_{16}Al$ compound.

Where Θ is the rescaled temperature, Tr1 and Tr2 are the temperatures of the two reference points that have been selected as those corresponding to $-\Delta S_{\rm M}=-a\times\Delta S_{\rm max}$ (where $0\leq a\leq 1$) [50].

It has been shown in some theoretical research that it is unnecessary to use two reference temperatures below and above T_C Tr1 and Tr2, but for a material with a single magnetic phase, only one Tr can be used. However, for materials with a significant demagnetization factor or multi-magnetic phases, two reference temperature points must be employed [51].

Fig. 17 shows that the normalized entropy change for all applied magnetic fields collapses in a single universal curve after rescaling temperature and choosing a=0.5. This suggests that $Pr_2Fe_{16}Al$ undergoes a second-order magnetic transition phase around T_C=356 K.

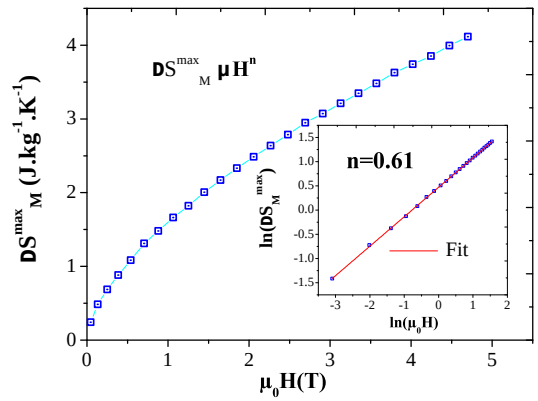

Figure 18. ΔS_M^{max} vs $\mu_0 H$. Inset show the same plot in a log-log scale.

Fig. 16 clearly shows that magnetic entropy change of $Pr_2Fe_{16}Al$ sample reaches its maximum around Curie temperature. The magnetic entropy maximum change depends strongly on the applied magnetic field. A non-linear relation can be expected between ΔS_M^{max} and $\mu_0 H$ as follows:

$$\Delta S_M^{max} \propto \mu_0 H^n$$

where n=2/3 in the case of mean-field model [52]. In order to predict the exponent n, which describes the dependence of magnetic entropy change at T=T_C for materials that do not follow the mean-field model in the critical regime, the equation of the Arrott-Noakes can be considered to describe the magnetic material around transition temperature. As described in Ref. [50], by differentiation and integration of the Arrott-Noakes equation, we can obtain a relation between n, β and γ:

$$n = 1 + \frac{\beta - 1}{\beta + \gamma} \tag{10}$$

By fitting the curve of the ΔS_M^{max} vs $\mu_0 H$, we obtain n=0.61

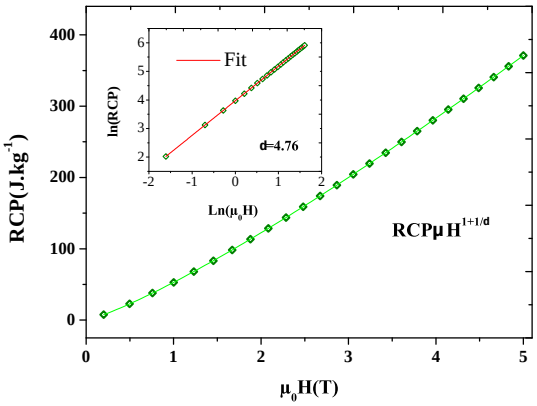

Figure 19. RCP vs $\mu_0 H$. Inset show the same plot on a log-log scale.

RCP variations with the applied magnetic field follow a power law, it is given by the following relation [53]:

$$RCP \propto H^{1+\frac{1}{\delta}} \tag{11}$$

Fig. 19 shows the variations of relative cooling power with the applied magnetic field, the fit gives δ=4.76 which is very close to the value obtained from the critical isotherm method. By the combination of the Eq. (10) and Widom scaling relation we obtain β and γ as follow:

$$\beta = \frac{1}{\delta(1-n)+1} \tag{12}$$

$$\gamma = \frac{\delta - 1}{\delta(1-n)+1} \tag{13}$$

The values of β, γ and δ determined from magnetocaloric method are listed in Tab. II for comparison. The critical exponents determined from the conventional methods are close to that found from the magnetocaloric method, which implies that the MCE method is helpful to study the critical behavior. Also, this agreement demonstrates the correlation between magnetic entropy change around Curie temperature and the universality class of magnetocaloric compounds.

7. *Interaction change distance*

It is essential to have a better idea of the nature and extent of the interaction in the material. Fisher *et al.* have in theoretical studies treated this type of magnetic order as an attractive interaction of spins, where analysis of renormalization group theory suggests that the interaction degrades with distance r as $J(r) = r^{-(3+\sigma)}$, where σ is a positive constant [54]. Moreover, the susceptibility exponent γ is predicted as:

$$\gamma = 1 + \left(\frac{4}{d}\right)\left(\frac{n+2}{n+8}\right)\Delta\sigma + \frac{8(n+2)(n-4)}{d^2(n+8)^2} \times \left[1 + \frac{2(G(\frac{d}{2})(7n+20)}{(n-4)(n+8)}\right]\Delta\sigma^2 \quad (14)$$

Where $\Delta\sigma = (\sigma - d/2)$, n is the spin dimensionality. In order to find the appropriate model that can reproduce the values of critical exponents found by using the conventional experimental methods (Modified Arrott plot, Kouvel-Fisher method, and critical isotherm), we used all possible combinations of d and n, for each couple d and n, we search σ value that gives γ values determined from conventional methods. Tab. III shows the values of σ, β and α obtained for different couples of d and n.

Table III. Values of σ, β and α with different combination (d, n) for $Pr_2Fe_{16}Al$ compound

d	n	σ	β	ν	α	δ
3	1	2.04	0.317	0.66	0.02	5.24
	2	1.96	0.362	0.68	-0.04	4.71
	3	1.90	0.388	0.70	-0.1	4.46
2	1	1.34	0.395	1	0	4.40
	2	1.29	0.369	1.04	-0.08	4.64
	3	1.26	0.329	1.07	-0.14	5.09
1	1	0.67	0.333	2.01	-0.01	5.03
	2	0.64	0.373	2.10	-0.1	4.61
	3	0.63	0.398	2.13	-0.13	4.38

According to this model, the range of spin interaction is long or short depending on $\sigma < 2$ or $\sigma > 2$. In fact,when $\sigma > 2$ the 3D Heisenberg model is valid, $J(r)$ decays faster then r^{-5} with short range type interaction, considering that $\sigma < 2$ it agrees with mean field model and $J(r)$ decays slower than $r^{-4.5}$. In the range between short range and long range $(1.5 < \sigma < 2)$ $J(r)$ decays slower then r^{-5} and faster than $r^{-4.5}$, the critical exponents take intermediate values between tow classes.

According to scaling equations we can obtain the values of ν, α, β and δ: $\nu = \gamma/\sigma$, $\alpha = 2 - \nu d$ and $\beta = (2 - \alpha - \gamma)/2$ [55, 56]. In our case for $Pr_2Fe_{16}Al$, we obtain ($\beta = 0.362$, $\gamma = 1.345$, and $\delta = 4.71$) which are the most closest values to our experimentally observed values. This calculation suggests that the spin interaction $Pr_2Fe_{16}Al$ is close to the Heisenberg [d : n] $\equiv$ [3 : 2] type coupled, the values of σ value is inferior to 2, suggesting the ferromagnetic interaction in this compound is long-range type interaction with $\sigma = 2.04$ and J(r) decays as $r^{-5.04}$ faster than $r^{-4.5}$.

IV. CONCLUSION

We have made a detailed study on the critical behavior in $Pr_2Fe_{16}Al$; our sample exhibits a second-order magnetic phase transition from the ferromagnetic state to the paramagnetic one. The critical exponents β, γ, and δ estimated from various conventional techniques are close and obey the scaling equation. Moreover, the determined critical exponents from the magnetocaloric method are consistent with those found from the modified Arrott plot method, Kouvel-Fisher method, and critical isotherm; this result supports using the MCE method to study the critical behavior. The determined exponents are close to 3D-Heisenberg ($d = 3 : n = 2$) spins coupled with a long-range interaction type ($\sigma = 1.96$), spin decays as $J(r) = r^{-4.96}$.

V. ACKNOWLEDGMENTS

This work was supported by the National Center for Scientific Research (CNRS), France, by the "Ministère de l'Enseignement Supérieur et de la Recherche Scientifique"(LMOP LR99ES17) Laboratory, Tunisia. The authors would like to acknowledge PRF2019-D4P2, PHC-Utique 21G1408, and Tuniso-Marrocain 20/R&D23

[1] S. Menouer, O. Miloud Abid, A. Benzair, A. Yakoubi, H. Khachai, and U. Schwingenschlögl. *Sci. Rep.*, 11(1):1–11, 2021.

[2] R.C. Das, A. Pathak, P. Bhorania, and M. Khan. *Bull.Aca.Sci.USSR.Phys*, 2021.

[3] A.N. Kazakov, D.V. Blinov, V.Yu. Bodikov, S.V. Mitrokhin, and A.A. Volodin. *Int. J. Hydrog*, 46(25):13622–13631, 2021.

[4] D. Zhang, S-J. Ji, and N-T. Suen. *ChemComm*, 57(68):8504–8507, 2021.

[5] H. Jaballah, W. Bouzidi, R. Fersi, N. Mliki, and L. Bessais. *J. Phys. Chem*, 161:110438, 2021.

[6] Z. Ma, X. Dong, Z. Zhang, and L. Li. *J. Mater. Sci. Technol.*, 92:138–142, 2021.

[7] D. Guo, L.M. Moreno-Ramírez, C. Romero-Muñiz, Y. Zhang, J-Y. Law, V. Franco, J. Wang, and Z. Ren. *Sci. China Mater*, 64(11):2846–2857, 2021.

[8] Y. Zhang, Y. Tian, Z. Zhang, Y. Jia, B. Zhang, M. Jiang, J. Wang, and Z. Ren. *Acta Mater.*, 102:117669, 2022.

[9] Y. Zhang, J. Zhu, S. Li, J. Wang, and Z. Ren. *J. Mater. Sci. Technol.*, 102:66–71, 2022.

[10] L. Li and M. Yan. *J. Alloys Compd*, 823:153810, 2020.

[11] Y. Zhang. *J. Alloys Compd*, 787:1173–1186, 2019.

[12] Y. Wang G. Yaming, D. Guo, B. Wu, S. Geng, and Y. Zhang. *J. Magn. Magn. Mater.*, 498:166179, 2020.

[13] Y. Zhang, B. Wu, D. Guo, J. Wang, and Z. Ren. *Chin. Phys. B*, 30(1):017501, 2021.

[14] P. Xu, Z. Ma, P. Wang, H. Wang, and L. Li. *Mater. Today Phys.*, 20:100470, 2021.

[15] Y. Zhang, J. Zhu, S. Li, Z. Zhang, J. Wang, and Z. Ren. *Sci. China Mater.*, pages 2199–4501, 2022.

[16] J. Fan, C. Huang, H. Liu, Y-E. Yang, JLS. Llamazares, CFS. Valdés, P. Gorria, C. Ma, Y. Zhu, and H. Yang. *CrystEngComm*, 23(18):3411–3418, 2021.

[17] L. Zhang, B. Wang, Y. Sun, P. Tong, J. Fan, C. Zhang, L. Pi, and Y. Zhang. *Phys.Rev.B*, 85(10):104419, 2012.

[18] A.K. Pramanik and A. Banerjee. *Phys.Rev B*, 79(21):214426, 2009.

[19] L. Xu, J. Fan, W. Sun, Y. Zhu, D. Hu, J. Liu, Y. Ji, D. Shi, and H. Yang. *Appl. Phys. Lett*, 111(5):052406, 2017.

[20] Yu. Liu, NV. Ivanovski, and C. Petrovic. *Phys.Rev B*, 96(14):144429, 2017.

[21] H. Jaballah, K. Nouri N. Mliki, L. Bessais, and M. Jemmali. *Chem. Phys. Lett.*, 787:139260, 2021.

[22] W.Ostertag and KL. Strnat. *Acta Crystallogr.*, 21(4):560–565, 1966.

[23] Z.W. Li and A. H. Morrish. *Phys. Rev. B.*, 55(6):3670, 1997.

[24] R. Guetari, R. Bez, A. Belhadj, K. Zehani, A. Bezergheanu, N. Mliki, L. Bessais, and C. B. Cizmas. *J. Alloys Compd.*, 588:64–69, 2014.

[25] L. Bessais, E. Dorolti, and C. Djega-Mariadassou. *Appl. Phys. Lett.*, 87, 2005.

[26] S. Khazzan, N. Mliki, L. Bessais, and C. Djega-Mariadassou. *J. Magn. Magn. Mater.*, 322(2):224–229, 2010.

[27] R. Bensalem, W. Tebib, S. Alleg, J. J. Sunol, L. Bessais, and J. M. Greneche. *J. Alloys Compd.*, 471:24–27, 2009.

[28] A. Hamrita, Y. Slimani, M. K. Ben Salem, E. Hannachi, L. Bessais, F. Ben Azzouz, and M. Ben Salem. *Ceram. int.*, 40:1461–1470, 2014.

[29] H. Rietveld. *Acta Crystallogr.*, 22:151, 1967.

[30] H. Rietveld. *J. Appl. Crystallogr.*, 2:65, 1969.

[31] J. Rodriguez-Carvajal. *Physica B* , 192:55, 1993.

[32] J. Rodriguez-Carvajal, M. T. Fernandez-Diaz, and J. L. Martinez. *J. Phys.* , 81:210, 2000.

[33] A. K. Pramanik and A. Banerjee. *J. Phys: Condens. Matter*, 20(27):275207, 2008.

[34] Qu. Johnson, D.H. Wood, G.S. Smith, and A.E. Ray. *Acta Crys B*, 24(2):274–276, 1968.

[35] G Calestani, N Magnani, A Paoluzi, L Pareti, and C Rizzoli. *Physical Review B*, 68(5):054424, 2003.

[36] P. Gorria, P. Alvarez, J. Sanchez Marcos, J. Sanchez-Llamazares, M. J. Perez, and J. A. Blanco. *Acta Mater.*, 57:1724–1733, 2009.

[37] L. Bessais, C. Djega-Mariadasso, D.K. Tung, and W. Hong N.X. Phuc. *J. Alloys Compd.*, 455(1-2):35–41, 2008.

[38] B.K Banerjee. *Physics letters*, 12(1):16–17, 1964.

[39] A. Arrott. *Phys Rev*, 108(6):1394, 1957.

[40] A. Arrott and J.E. Noakes. *Phys. Rev. Lett.*, 19(14):786, 1967.

[41] S. N. Kaul. *J. Magn. Magn. Mater.*, 53(1-2):5–53, 1985.

[42] A.K. Pramanik and A. Banerjee. *Phys. Rev. B*, 79(21):214426, 2009.

[43] M. E. Fisher. *Rep. Prog. Phys.*, 30(2):615, 1967.

[44] M. E. Michael J.S. Kouvel. *Phys. Rev*, 136(6A):A1626, 1964.

[45] M. Haug, M. Fähnle, H. Kronmüller, and F. Haberey. *J. Magn. Magn. Mater*, 69(2):163–170, 1987.

[46] M. Dudka, R. Folk, Yu. Holovatch, and D. Ivaneiko. *J. Magn.Magn. Mater., 256, 243*, 2003.

[47] M. Foldeaki, R. Chahine, and T. K. Bose. *J. Appl. Phys.*, 77:3528, 1995.

[48] S. Fujieda A. Fujita and K. Fukamichi. *J. Magn. Magn.Mater.*, 2007.

[49] A. Das and A.K. Majumdar. *J. Magn. Magn. Mater*, 128(1-2):47–57, 1993.

[50] V. Franco, J. S. Blázquez, and A. Conde. *Appl. Phys. Lett.*, 89(22):222512, 2006.

[51] V. Franco and A. Conde. *J. Int. Acad. Refrig.*, 33(3):465–473, 2010.

[52] M. Seeger, S.N. Kaul, K. Kronmüller, and R. Reisser. *Phys. Rev. B*, 51(18):12585, 1995.

[53] Y. Su, Y. Sui, J-G. Cheng, J-S. Zhou, X. Wang, Y. Wang, and J.B. Goodenough. *Phys. Rev. B*, 87(19):195102, 2013.

[54] M.E. Fisher, S-K. Ma, and B. G. Nickel. *Phys Rev Lett*, 29(14):917, 1972.

[55] J.C. Le Guillou and J. Zinn-Justin. *Phys. Rev. B 21, 3976*, (1980).

[56] M. E. Fisher. *Rev. Mod. Phys. 46, 597*, (1974).